*Geotechnical Testing Journal*, Vol. 32, No. 5
Paper ID GTJ102154
Available online at: www.astm.org

*S. Thevanayagam,[1] T. Kanagalingam,[1] A. Reinhorn,[1] R. Tharmendhira,[1] R. Dobry,[2] M. Pitman,[1] T. Abdoun,[2] A. Elgamal,[3] M. Zeghal,[2] N. Ecemis,[4] and U. El Shamy[5]*

# Laminar Box System for 1-g Physical Modeling of Liquefaction and Lateral Spreading

**ABSTRACT:** Details of a large scale modular 1-g laminar box system capable of simulating seismic induced liquefaction and lateral spreading response of level or gently sloping loose deposits of up to 6 m depth are presented. The internal dimensions of the largest module are 5 m in length and 2.75 m in width. The system includes a two dimensional laminar box made of 24 laminates stacked on top of each other supported by ball bearings, a base shaker resting on a strong floor, two computer controlled high speed actuators mounted on a strong wall, a dense array advanced instrumentation, and a novel system for laboratory hydraulic placement of loose sand deposit, which mimics underwater deposition in a narrow density range. The stacks of laminates slide on each other using a low-friction high-load capacity ball bearing system placed between each laminate. It could also be reconfigured into two smaller modules that are 2.5 m wide, 2.75 m long, and up to 3 m high. The maximum shear strain achievable in this system is 15 %. A limited set of instrumentation data is presented to highlight the capabilities of this equipment system. The reliability of the dense array sensor data is illustrated using cross comparison of accelerations and displacements measured by different types of sensors.

**KEYWORDS:** sand, liquefaction, lateral spreading, physical modeling, earthquake

## Introduction

Liquefaction of loose saturated granular soil and liquefaction-induced lateral spreading of gently sloping ground near waterfronts are major causes of geotechnical damage to buildings, bridges, port facilities, and other pile-supported structures during earthquakes (McCulloch and Bonilla 1970; Hamada et al. 1986; Mizuno 1987; Hamada and O'Rourke 1992; O'Rourke and Hamada 1992; Bartlett and Youd 1992; Youd 1993; Swan et al. 1996; Ishihara et al. 1996; Tokimatsu et al. 1996; Berrill et al. 1997; Yokoyama et al. 1997; Tokimatsu 1999; Dobry and Abdoun 2001; Koyamada et al. 2005; Lin et al. 2005). Effects of liquefaction and lateral spreading on foundations have been studied using simplified semi-empirical theories, advanced numerical models, a limited number of large scale 1-g shaking table tests (Suzuki et al. 2005; Tamura and Tokimatsu 2005; Towhata et al. 2006; He et al. 2006), and centrifuge model tests (Dobry et al. 1995; Abdoun et al. 2003; Haigh and Madabhushi 2005; Brandenberg et al. 2005, 2007; Elgamal et al. 1996). A limited number of full scale field experiments have also been carried out utilizing blast-loading techniques to induce liquefaction and lateral spreading (Ashford et al. 2006). There has not yet been a study focusing on 1-g large scale liquefaction-induced lateral spreading to understand the major factors causing initiation of lateral spreading nor an integrated study involving large scale 1-g shake table testing, centrifuge testing, and numerical modeling techniques to understand liquefaction and lateral spreading phenomena and its effects on foundations. Recently a large scale research project has been initiated to study liquefaction-induced lateral spreading and its effects on pile foundations using all three approaches indicated above (Dobry et al. 2007; Dobry et al. 2009; Gonzalez 2008). As a part of this study, a large scale laminar box system has been developed to simulate liquefaction of saturated loose sands, under level ground conditions, as well as lateral spreading of saturated loose gentle slopes. It also involves a dense array of instrumentation to collect detailed data on the progression of liquefaction and lateral spreading phenomena. The dense array consists of various types of sensors each of which record acceleration, deformation, and pore pressures at the same or nearby locations. It allows one to cross check the measurements obtained by different types of sensors and verify the quality and reliability of the data.

This paper presents the salient features of this laminar box system and a limited set of liquefaction test results to illustrate the utility and versatility of the system. A separate paper (Thevanayagam et al. 2009) presents a detailed account of the liquefaction tests and an analysis of the test data illustrating the factors affecting the initiation of lateral spreading. Another paper (Dobry et al. 2009) presents a detailed analysis of the mechanics of liquefaction-induced lateral spreading based on the test data and observations. Comparative analysis of results from 1-g laminar box tests and centrifuge experiments (Gonzalez 2008) and numerical simulations of these tests are presented elsewhere (El Shamy et al. 2009).

Manuscript received September 30, 2008; accepted for publication June 19, 2009; published online August 2009.

[1]Dept. of Civil and Environmental Engineering, Univ. at Buffalo, 212 Ketter Hall, Buffalo, NY 14260, e–mail: theva@eng.buffalo.edu

[2]Dept. of Civil and Environmental Engineering, Rensselaer Polytechnic Institute, 110 8th Street, JEC 4049, Troy, NY 12180.

[3]Dept. of Structural Engineering, University of California, San Diego, MC-0085, La Jolla, CA 92093.

[4]Dept. of Civil Engineering, Izmir Institute of Technology, Turkey 35430.

[5]Dept. of Environmental and Civil Engineering, Southern Methodist University, P. O. Box 750340, Dallas, TX 75275.

## 1-g Laminar Box System

Figure 1 shows a schematic sketch of a 1-g geotechnical laminar box shaking system developed at the Network for Earthquake Engineering Simulations (NEES) facility at the University at Buffalo (UB). It has the capability to test up to nearly 80 $m^3$ of sand simulating a soil deposit of up to 6 m deep. It consists of (a) a laminar

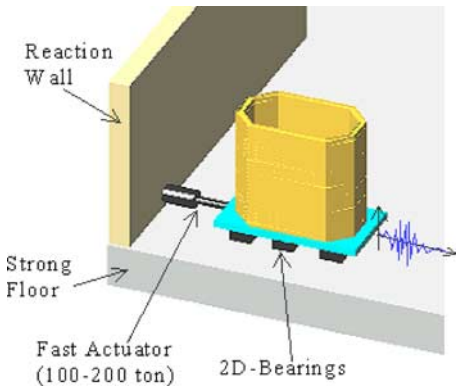


FIG. 1—*Large-scale geotechnical laminar box system.*

box capable of simulating two dimensional ground shaking in horizontal direction, (b) base-shaker system supported on a strong floor, (c) two high speed hydraulic actuators mounted on a strong reaction wall and attached to the base shaker, and (d) computer controlled system to provide any desired base motion to the actuators and base shaker. The system also consists of a robust laboratory hydraulic filling system for sand placement underwater, novel dense array instrumentation, high speed video cameras, and a high speed and time-synchronized data acquisition system to record all data with a common reference time frame and time interval.

## *Laminar Box*

Figure 2(*a*)–2(*c*) shows the schematic inner details of the laminar box. It is a stacked-ring system consisting of 24 octagon-shaped aluminum laminates (rings). The laminates are made of aluminum I-beams, each 0.25 m wide and 0.30 m deep (Fig. 2(*c*)). Aluminum was chosen to reduce the weight of the rings and its inertia effects on the soil inside during shaking. Each laminate, with all its components, weighs about 6.936 kN without soil. The ratio of ring weight to saturated soil weight in each ring is about 11 %. The rings are separated and supported by a number of distributed high capacity ball bearings placed between the laminates. The internal dimensions of the box are 5.0 m in length and 2.75 m in width. The maximum height of the box is 6.2 m when all 24 laminates are stacked together. The entire laminar box container is supported on a base-shaker system to which the input motions are applied through two high speed actuators. Figure 2(*a*) shows the plan view. Figure 2(*b*) shows the cross-section of the laminar box. Figure 2(*c*) shows a

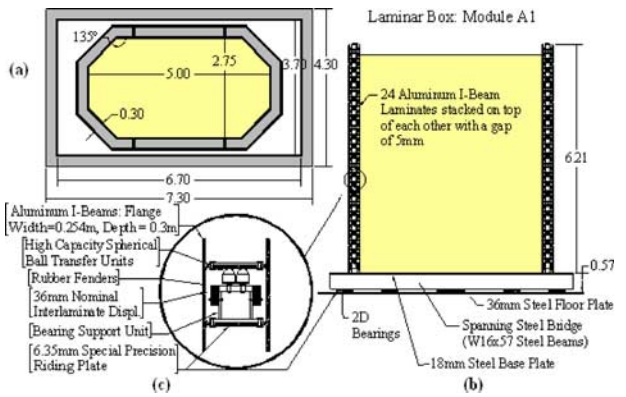


FIG. 2—*Schematic details of laminar box.*

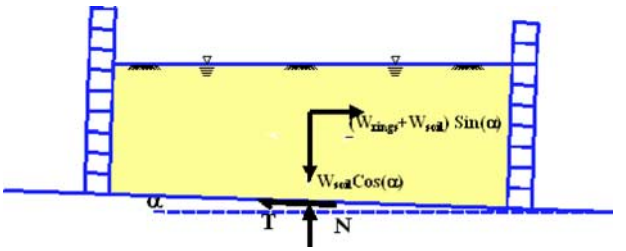


FIG. 3—*Inclined laminar box and equivalent slope.*

cross-section of the rings to illustrate the inner details of the ball bearings and the bearing support units. A total of 12 bearing support units, each containing four ball bearings (No. 21163, General Bearing, Inc.), is mounted inside the top channel of the I-beam in each laminate. The under side of the I-beams below the bearing support units are lined with steel hardened plates. When the laminates are stacked together they sit on each other resting on ball bearings. The ball units are leveled to make a planer surface and adjusted to be in contact with the hardened steel plate in the underside of the I-beam on top. The top heights of ball bearings are adjusted such that a small vertical gap (3–5 mm) is provided between the flanges of the I-beam laminates. The vertical gap is intended to prevent any contact interference between any adjacent laminates during horizontal sliding of the laminates. When the laminates slide with respect to one another, the ball bearing units ride on the steel hardened plates. The hardened plates and the ball transfer units are manufactured to a high standard to minimize indentations or rutting occurring along the travel paths during sliding. The coefficient of friction between the ball bearings and the hardened plate is nominally less than 0.5 %. Each laminate is allowed to slide horizontally a maximum of 36 mm in the longitudinal direction relative to the adjacent laminate. The maximum shear strain that a soil contained inside the box could be subjected to is 15 %. Horizontal displacements exceeding 36 mm may cause excessive stresses on the laminates and/or excessive overturning moments and cause instability. Safety precautions are incorporated in the design to address this, and they must be implemented carefully on a case-by-case basis (Bethapudi 2008).

## *Sloping Ground Conditions*

To simulate level ground conditions, the bearings are leveled horizontal in longitudinal and transverse directions. The laminates are stacked vertically on top of each other. The laminates can slide only in any horizontal direction. For cases where liquefaction and lateral spreading of gentle sloping ground inclined at an angle $\alpha_{field}$ is to be simulated, the base ring is inclined gently at an angle $\alpha_{box}$ horizontal in the longitudinal direction. The ground water is horizontal. The laminates are stacked vertically as above, but each laminate and the top surface of the ball bearings are inclined at an angle $\alpha_{box}$ horizontal in the longitudinal direction and leveled horizontal in the transverse direction. This allows the soil inside the box to slide along a plane inclined at $\alpha_{box}$ within the soil box should there be any sliding during experiments. However, the static shear stresses present along these planes are equal to that of an infinitely sloping submerged ground inclined at $\alpha_{field}$, much higher than $\alpha_{box}$.

As shown in Fig. 3, at any sliding plane at depth $z$ below the ground surface, the static shear stress along the sliding planes in the soil in the box is given by $\tau_{static} = T/A = (W \sin(\alpha_{(box)}))/A$, where $T$ = static driving shear force; $W$ = total weight of saturated soil ($W_{soil}$)

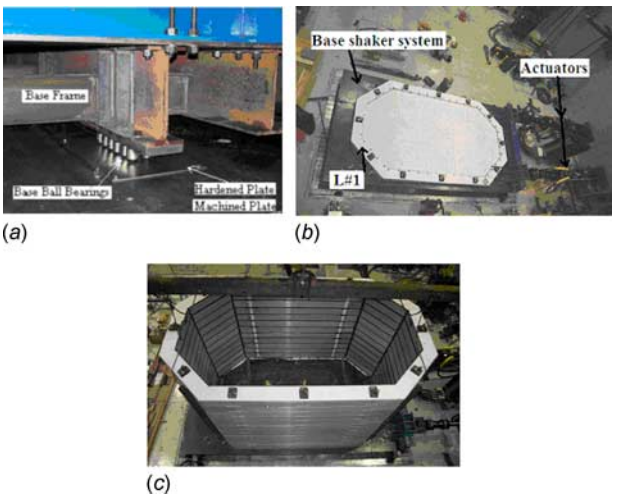


FIG. 4—*Laminar box components: (a) Base-shaker bearings; (b) base shaking system; and (c) actuator-shaking base-laminar box assembly.*

and rings ($nW_{ring}$) above the potential sliding plane=($W_{soil}+nW_{ring}$); $A$=area of soil; $n$=number of rings above depth $z$; and $W_{ring}$=weight of each ring. The shear stress ratio along these planes is $\tau_{static}/\sigma'_{no}=(W_{soil}+nW_{ring})\tan(\alpha_{box})/(W'_{soil})$, where $\sigma'_{no}$=effective stress normal to the sliding plane, and $W'_{soil}$=submerged weight of the soil. For an infinitely sloping submerged ground with horizontal water level, sliding at an angle $\alpha_{field}$, the stress ratio is given by $\tau_{static}/\sigma'_{no}=\tan\alpha_{field}$ (Lambe and Whitman 1969). Equating the static shear stress ratios, $\tan(\alpha_{field})=(W_{soil}+nW_{ring})\tan(\alpha_{box})/(W'_{soil})$. A gentle 2° inclination of this box in the laboratory is equivalent to simulating a field slope $\alpha_{field}$ of 4.5° ~ 5.0°. Similar corrections have been proposed for centrifuge modeling experiments as well involving inclined laminar box to simulate sloping ground conditions (Taboada 1995; Dobry and Taboada 1994; Taboada and Dobry 1994).

## *Base Shaker*

The base-shaker system consists of a horizontal steel base frame with a flat and horizontal steel plate mounted on top of it. The first laminate (bottom ring) is tied to the steel plate on top of the steel frame. The under side of the steel frame has a series of distributed ball bearing units. The ball bearings rest on hardened steel plates mounted on a 36 mm thick machined steel base plate tied tightly to the strong floor inside the NEES laboratory (Fig. 4(*a*)–4(*c*)). The strong floor has a very high-load carrying capacity far exceeding the weight of the laminar box and soil, but not unlimited. The 36 mm base plate is leveled to be horizontal. The ball units are adjusted to be in contact with the hardened plates at all times. Figure 4(*b*) shows the base shaking unit with the first laminate (bottom ring) tied to it. Figure 4(*c*) shows the entire laminar box stacked on the base shaking unit. A 1.1 mm thin rubber membrane bag is placed inside the box to contain the soil within the box. The total weight of the laminar box, including the shaking base and the soil inside it at its full capacity, is in the vicinity of about 1600 kN. The relative density of sands to be tested in this apparatus ranges from very loose to loose.

## *Base Shaking Controls*

The intended maximum horizontal shaking intensity is 0.3 g. Two computer controlled high speed MTS actuator systems, each capable of 900 kN, mounted on a strong reaction wall and tied to the base shaking frame are used to precisely control the actuators and the input base motions. The actuators are force powered by four MTS pumps each rated at 12 L/s flow capacity at 20.7 MPa working pressure. The actuators can be fed with any recorded earthquake ground motion or any synthetic motion and the controllers can be calibrated to compensate for compliance effects to accurately shake the base of the soil to any given specific input ground motion. In order to minimize any transverse shaking of the base shaker and guide the base shaker in the longitudinal direction, four spring-loaded restrainer guide blocks were placed at the corners of the base shaker. This will only help guide the base shaker in the longitudinal direction. No external lateral structural frames or motion restrainers are present to limit the lateral motion of the laminates in this configuration. Horizontal safety cables with pre-set travel lengths are installed at five different laminate levels and tied to the strong wall to limit excessive longitudinal movement of the laminates should the interlaminate displacements exceed 36 mm (Fig. 5(*a*)–5(*c*)). An external frame and additional internal motion restraint systems are possible, and they are considered as part of future modifications to the system (Bethapudi 2008). At the present configuration, no further restrainers other than loose vertical cables with pre-set travel length limits (Fig. 5(*d*)) is used to limit possible uplifting of the laminates. This is a limitation of the apparatus if large complementary vertical shear stresses are to be resisted during shaking. The self weight of the laminates is the limiting vertical force in this case. This is not a serious limitation for testing loose sand that liquefies under relatively small shear stresses and small excitations. Where large vertical shear stresses are anticipated, vertical uplift restrainers must be incorporated as part of future modification to this system (Bethapudi 2008). Additional safety measures are implemented on a case-by-case basis.

Although Figs. 2 and 3 show only one configuration, the laminar box is designed to be modular. The box can be reconfigured to obtain two smaller laminar boxes that are 2.5 m wide, 2.75 m long, and 3 m high each, allowing this box to be versatile and scalable to study a host of problems. Smaller sizes allow it to be used by placing them on one or two existing standard 6 degrees of freedom shake tables available at University at Buffalo (UB) NEES, each with a nominal payload capacity of 50 tons at a shaking intensity of 0.3 g. The shake tables can be relocated apart up to a distance of 35 m. For example, such small size configurations may be placed on two separate shake tables, spaced apart, to provide foundations for a bridge segment and simulate soil-foundation-structure interaction responses.

## *Hydraulic Filling*

A robust hydraulic pumping and sand placement method was developed to transfer sand in a slurry form from storage and to build soil deposit inside the laminar box. It allows sand grains to slowly settle down through water, mimicking natural alluvial deposition of sands in rivers, lakes, or man-made port islands. It involves a closed-loop hydraulic slurry pumping system (Fig. 6). This method also has the advantage of maintaining dust-free environment inside the laboratory populated with sensitive electronic equipment, actuators, and sensors systems. A 6.35 cm diameter slurry hose attached to a three-phase 5 hp slurry pump is used to pump the slurry from a sand storage tank. A diffuser, attached to the outlet of the slurry hose, disperses the slurry as it exits. The slurry hose is moved longitudinally along the box back and forth using an over-

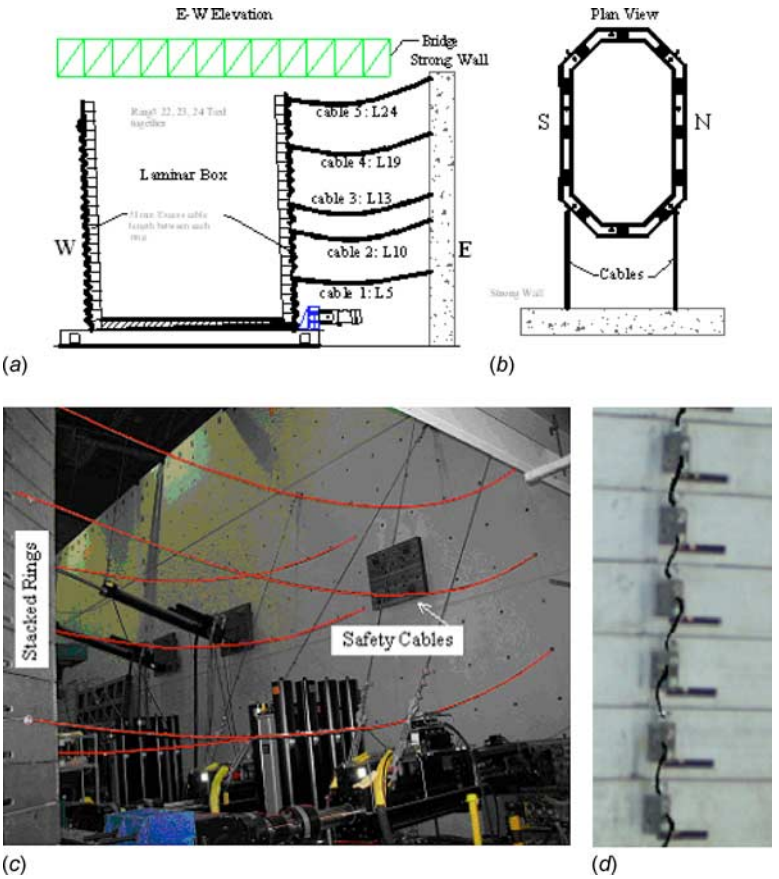


FIG. 5—*Safety cables: (a) Schematic diagram, side view; (b) schematic diagram, plan view; (c) horizontal safety cables; and (d) vertical cables.*

head crane to uniformly place sand throughout the laminar box. A return water hose powered by two 5 hp trash-water pumps (Honda WT20) is used to return the excess water from the laminar box to the slurry tank. The pumping is adjusted to maintain a certain height of water above the sand surface inside the laminar box. The relative density of the soil achieved inside the laminar box depends on a number of factors including the slurry solid content, discharge velocity, slurry discharge direction, discharge height above water level inside the laminar box, and height of free standing water above sand surface inside the box. During trial tests using Ottawa sand F-55 (Fig. 7), these parameters were varied to determine these parameters to obtain a desired density. These experiments showed that a relative density of 30–40 % could be achieved by maintaining 0.6 m of water above the sand and maintaining the diffuser pipe discharging slurry horizontally at 0.3 m above the water. During the entire operation, continued monitoring of the above parameters is required for quality control. It takes about 4–5 days to fill the full height of the box. Several 15 cm diameter and 15 cm high steel buckets are placed inside the laminar box prior to filling and removed as the hydraulic fill sand surface reaches the top of the buckets. The in situ density is monitored using these bucket density data.

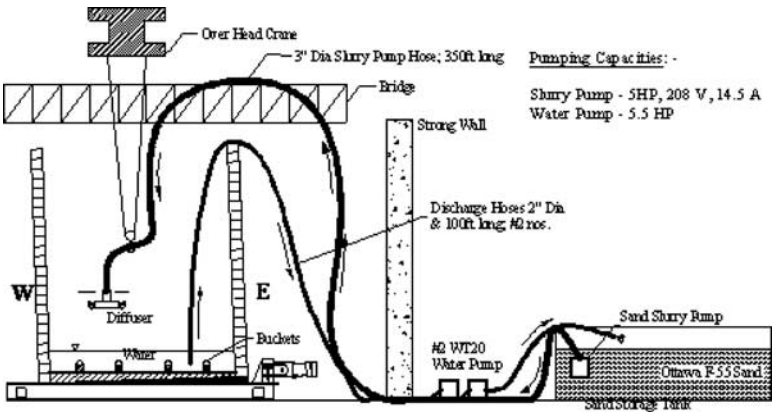


FIG. 6—*Closed-loop hydraulic filling.*

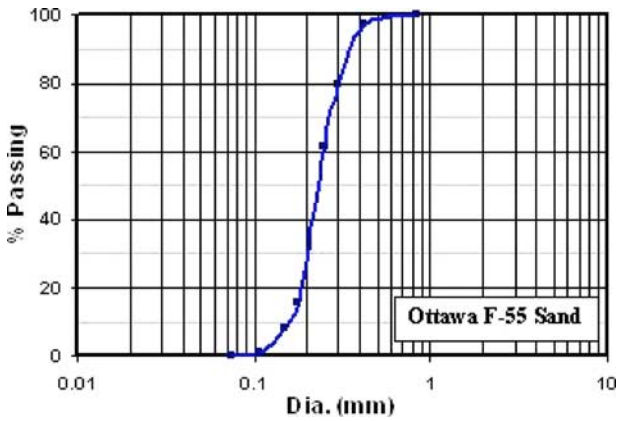


FIG. 7—*Gradation of Ottawa F-55 sand.*

Indirect relative density values obtained using correlations between cone penetration resistance and relative density (Schmertmann 1976; Jamiolkowski et al. 2001) are also determined using cone penetration tests (CPTs) at the end of hydraulic fill placement. They are used to monitor the consistency of the fill. A system identification technique (Zeghal and Elgamal 1994) based on soil response when the laminar box is subjected to very low level of shaking excitation at its base is also used to determine the shear wave velocity profile of the deposit.

## *Instrumentation*

Table 1 shows the type of sensors used for laminar box tests and details about the manufacturers. The instrumentation includes a dense array of traditional accelerometers, pore pressure transducers, displacement gages (potentiometers), and high speed digital video cameras. In addition, shape-acceleration arrays (SAAs) (Measurand Corp., Canada) consisting of micro electro mechanical system (MEMS) sensors packaged in a flexible hardened rubber tube with sensors spaced 0.3 m apart is also used (Fig. 8). SAA sensors record triaxial accelerations, displacements, and rotations at each sensor location (Abdoun and Danisch 2005; Abdoun et al. 2008; Bennett et al. 2009). The instrumentation sensors that are installed inside the soil includes SAA sensors, submersible accelerometers, and pore pressure transducers. These instruments are placed inside the laminar box before the sand placement by hanging the instruments from a bridge (Fig. 6) located vertically above the laminar box. The accelerometers are sealed in wax to water proof them and have a bulk density nearly the same as that of the soil so that they do not sink or float during liquefaction. The orientation of the accelerometers are carefully maintained in $x$ or $y$ direction as appropriate. The SAAs are installed with the bottom of the SAA tube fixed to the base shaker from inside the laminar box. In this case, the first laminate of the laminar box is rigidly tied to base shaker. The SAA is tied to the first laminate. It is then loosely hung from a bridge above the box. Figure 9 shows a typical instrumentation setup inside the laminar box. Some potentiometers are installed on the top soil surface. These potentiometers are attached to a wooden plate with steel weights attached to it to bring the bulk density to that of soil to prevent it from sinking or floating during testing. The primary objective of these potentiometers is to measure vertical settlement of ground surface. A third set of instrumentation includes accelerometers and potentiometers attached to the outside wall on the laminates. A fourth set of sensors includes high speed digital video cameras strategically placed to monitor critical components or portions of the laminar box from above and from various directions at ground level. All sensors are synchronized to a common clock and data are recorded in a common data acquisition system (Pacific Instruments, 6000 Data Acquisition Mainframe, California) with a maximum capacity of 256 channels at 128 Hz frequency. The SAA data are recorded separately, synchronized to the same common clock. This time-synchronization allows 3D viewing of the sensor response data and analyses of the response of the soil as a whole. A 3D viewer is available at Rensselaer Polytechnic Institute (RPI) (http://it.nees.org/about/community/archives/guest_feature/rpi-3d-visualization-tools.php) (Radwan and Abdoun 2006).

TABLE 1—*SG-1 Instrument notations, quantity, and their models.*

| Instruments | No. of Sensors | | Model |
|---|---|---|---|
| | LG-0 | SG-1 | |
| 3D – SAA | 2 sets (288 sensors) | 2 sets (315 sensors) | ShapeAccelArray MEMS Sensors |
| Piezometers | 13 | 20 | GE Druck Model PDCR 81 |
| X-Acc (Ring and Base) | 21 | 25 | Sensotec 10G |
| Y-Acc (Ring and Base) | 12 | 14 | |
| Soil-Acc-x | 5 | 6 | |
| Soil-Acc-y | 3 | 3 | |
| X-Potentiometers | 18 | 11 | MTS Temposonic Displacement Transducers |
| Z-Potentiometers | 3 | 3 | |
| Video Camera | 4 | 4 | |

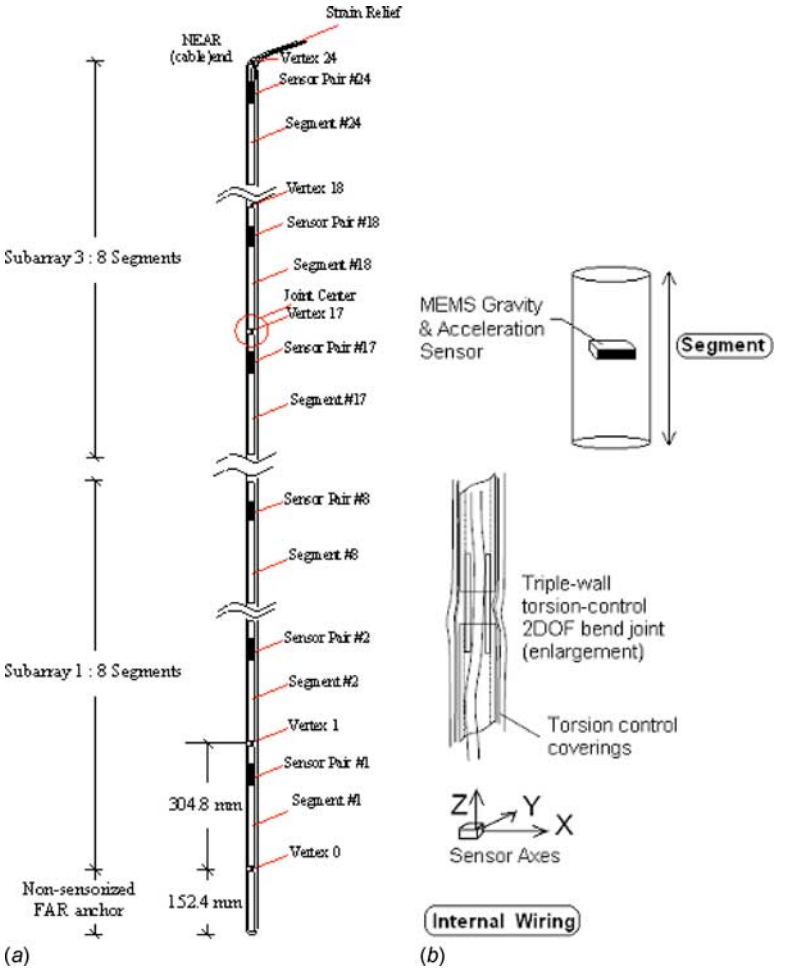


FIG. 8—*High-Bandwith ShapeAccelArray sensor internal components: (a) SAA internal components and dimensions; (b) internal components of each segment.*

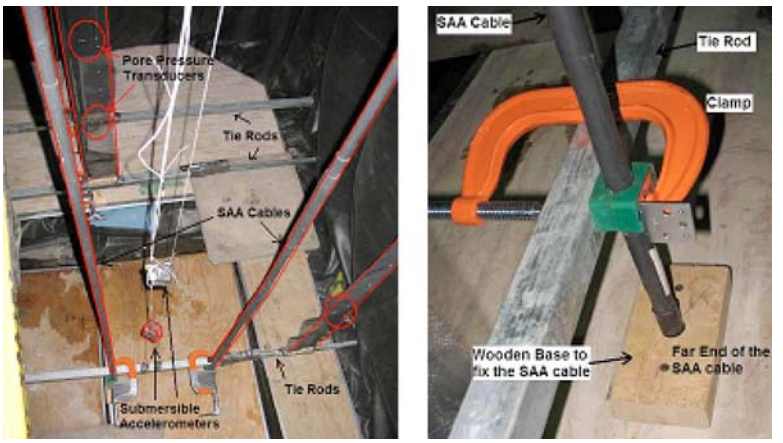


FIG. 9—*Instrumentation setup inside the laminar box.*

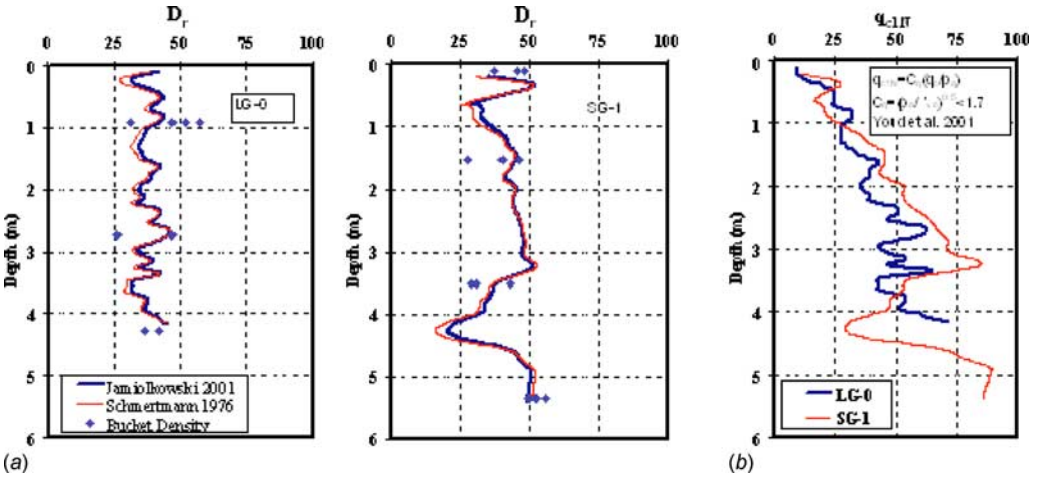


FIG. 10—*(a) Relative density; (b)* $q_{c1N}$.

## Shaking Tests

### *Soil Preparation*

Two shake tests were conducted using the above laminar box system. The first test involved a level ground, called LG-0. It was intended to evaluate the response of the laminar box system and its capability to simulate large scale liquefaction when filled with saturated loose sand and subjected to progressively increasing base shaking. The second test involved a gently sloping ground, named SG-1, to study liquefaction-induced lateral spreading of soils when subjected to shaking. The laminar box for SG-1 was inclined at $\alpha_{box}=2°$ horizontal in the longitudinal direction. It simulated the response of an infinitely sloping submerged ground inclined at $\alpha_{field}=4.6–5°$.

Soil deposits were constructed inside the laminar box using hydraulic filling method using Ottawa sand F-55. Undrained monotonic and cyclic triaxial compression test data for this sand is published elsewhere (Thevanayagam et al. 2002, 2003; Thevanayagam 2007a, 2007b). The soil depth in LG-0 was 5 m, whereas it was 5.6 m in SG-1. Figure 10(*a*) shows the relative density profiles for LG-0 and SG-1, respectively. In situ CPTs were done using standard cone penetrometer (ASTM D3441) with cone diameter of 4.37 cm. Cone penetration rate ranged between 2.0 and 3.7 cm/s. The relative density profiles were obtained using bucket density test data and from the relative density correlations based on cone penetration resistance (Schmertmann 1976; Jamiolkowski et al. 2001):

$$D_r = \frac{1}{C_2}\ln\left[\frac{q_c/P_a}{C_0(\sigma_v'/P_a)^{C_1}}\right] \tag{1a}$$

$$D_r = A_o + B_o^* \ln\left[\frac{q_c}{(\sigma_{vo}')^{\alpha}}\right] \tag{1b}$$

where:

the non-dimensional factors $C_o, C_1, C_2=17.68$, 0.50, and 3.1, respectively (Schmertmann 1976);

$D_r$=decimal relative density;

$\sigma_v'$=effective overburden stress; and

$P_a$=atmospheric pressure expressed in the same units as that of $\sigma_v'$ and penetration resistance $q_c$.

For Eq 1b, the values of $A_o$, $B_o$, and $\alpha$ are −1.292, 0.268, and 0.52, respectively (Jamiolkowski et al. 2001; Lancellotta 1983), and $q_c$ and $\sigma_{vo}'$ are in kPa. Figure 10(*b*) shows the normalized cone penetration resistance $q_{c1N}$ profiles for LG-0 and SG-1, respectively. $q_{c1N}$ was obtained based on measured tip resistance $q_c$ using (Youd et al. 2001):

$$q_{c1N} = \frac{q_{c1}}{p_a} = c_q\left(\frac{q_c}{p_a}\right) \tag{2a}$$

$$c_q = \left(\frac{p_a}{\sigma_{vo}'}\right)^n < 1.7 \tag{2b}$$

where:

$n$=0.5 for clean sand;

$\sigma_{vo}'$=effective vertical stress in the same units as $p_a$;

$q_{c1}$=normalized CPT tip resistance corrected for effective overburden stresses corresponding to 1 ton/ft$^2$ (100 kN/m$^2$); and

$p_a$=1 atm pressure in the same units used for $q_c$.

Figure 11(*a*) shows the instrumentation plan for LG-0. The instrumentation plan for SG-1 is nearly the same as in LG-0 (Bethapudi 2008).

The soil profiles determined using field density tests and static CPT are very consistent and indicate on the average, a relative density, $D_r \approx 40$ %, and a normalized cone penetration resistance, $q_{c1N} \approx 50$. Based on system identification techniques using soil response subjected to small amplitude, shaking excitation of the deposit indicated a normalized shear wave velocity of approximately $V_{s1} \approx 115$ m/s (Dobry et al. 2009). These values indicate that the soil deposits tested are representative of many of the loosest and most liquefiable, hydraulically deposited, geologically young saturated sand layers encountered in seismic areas around the world.

### *Base Shaking*

The base motion used for both tests is shown in Fig. 12. First 5 s (ten cycles) of motion consists of a 0.01 g amplitude shaking, which is termed as the non-destructive (ND) shaking. The ND motion was intended to shake the soil at small strain levels without causing rise in pore water pressures and use the measured acceleration data to obtain low strain shear modulus and shear wave velocity profile of the soil deposit using system identification techniques

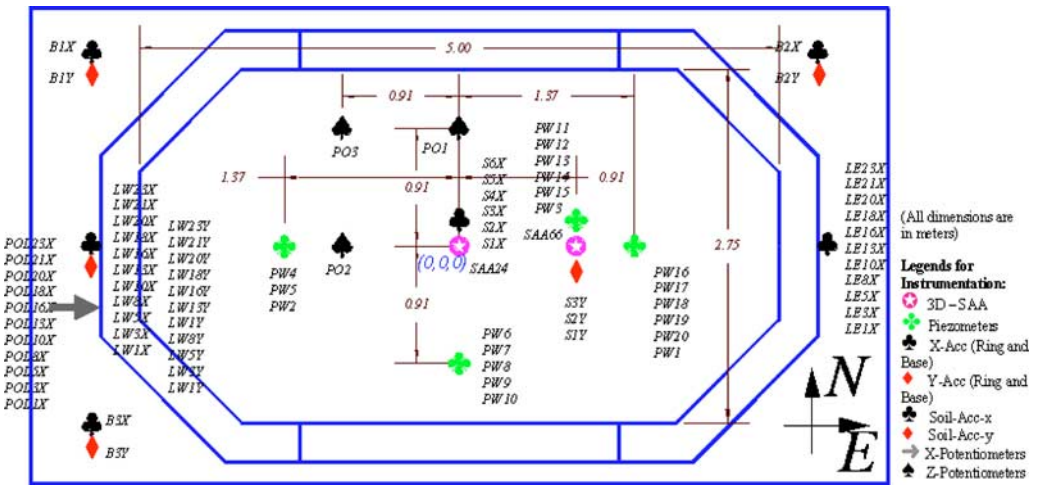


FIG. 11—*Instrumentation plan: LG-0 (plan view only) (additional details are available in Bethapudi 2008).*

(Zeghal and Elgamal 1994). Subsequent motion consists of three subsets of motions of 10 s duration each (20 cycles each, 2 Hz frequency) with amplitudes of 0.05, 0.15, and 0.3 g, respectively. The full duration of shaking was carried out for test LG-0. A computer controlled feedback system was used to control base shaking as close as possible to the intended motion shown in Fig. 12. However, for SG-1, the shaking motion was stopped after 8.4 s because of excess deformations in the soil. In each case, the base accelerations were recorded at three different locations B1, B2, and B3 (Fig. 11) on the base shaker to verify the input motions.

## Results

### *Accelerations*

Figure 13(*a*) shows the recorded base acceleration histories in the longitudinal direction recorded at three different locations at the base in LG-0. *X* refers to longitudinal direction and *Y* refers to transverse direction. Figure 13(*b*) shows the ratios of peak amplitudes of transverse accelerations $a_y$ divided by peak accelerations in the longitudinal direction $a_x$, recorded during each of the four different shaking durations: 0–5, 5–15, 15–25, and 25–35 s. The transverse accelerations are significantly lower than longitudinal accelerations throughout the shaking duration. This indicates that the base-shaker system was essentially functioning well providing shaking in the longitudinal direction with very little transverse components. Figure 14(*a*) and 14(*b*) shows the longitudinal acceleration histories of the laminates at various depths for LG-0 and SG-1, respectively.

### *Pore Pressures, Lateral Deformations, and Settlements*

Figure 15(*a*) and 15(*b*) shows the excess pore pressure response at three depths for LG-0 and SG-1. The data for LG-0 also include post-shaking pore pressure dissipation data. In both cases, it is clear that a significant portion of the soil in the laminar box did reach liquefaction. The pore pressures reached values approaching effective overburden stress at each depth. Figure 15(*a*) shows a classical example of typical time history response for excess pore water generation up to the end of shaking and dissipation and upward migration of pore water after the end of shaking. Dissipation of pore water pressure begins early at the bottom layer followed by delayed pore pressure dissipation in the top layers due to water migration from bottom to top, which helps delay dissipation of pressures in the top layers. In the case of SG-1, excessive lateral spreading displacements (Fig. 16) had reached intolerable limits and the laminar box and instrumentation was damaged after 8.4 s (Bethapudi 2008).

Figure 17 shows the ground surface settlement data for LG-0 during and shortly after shaking with time at three different locations in the ground surface. The total settlement was around 100 mm, of which 40 mm occurred during shaking and the rest as the pore pressure dissipated.

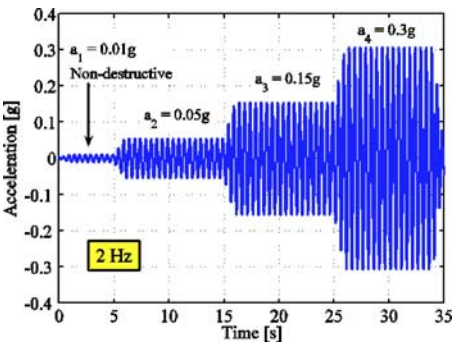


FIG. 12—*Input ground motion.*

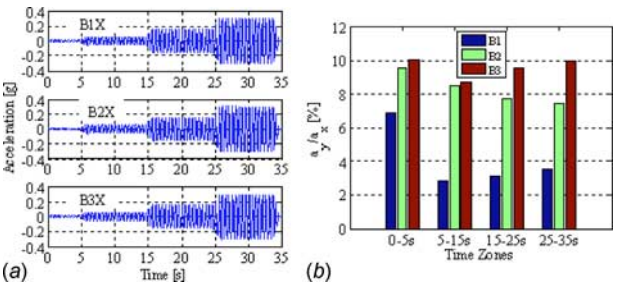


FIG. 13—*Recorded base acceleration: LG-0: (a) X-accelerations; (b) ratio of the amplitudes of $a_y/a_x$.*

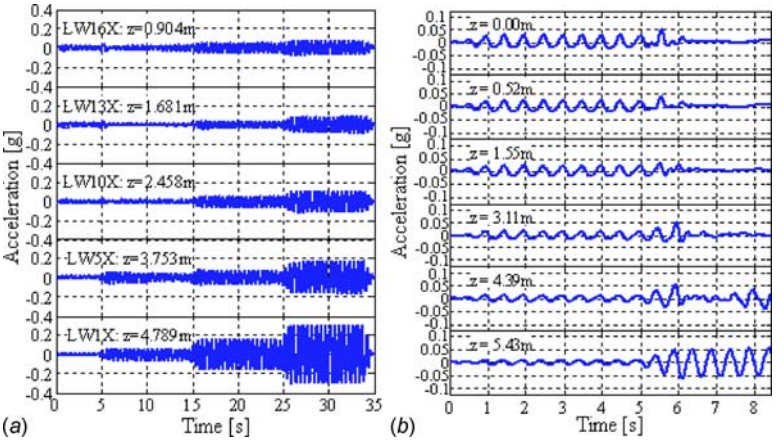


FIG. 14—*Acceleration: (a) LG-0; (b) SG-1.*

## *Cross-Comparison Between Sensors*

In order to assess the reliability of the sensor data, the data from different types/brand of sensors measuring displacements and accelerations were compared. This included a comparison of (a) acceleration histories measured by traditional accelerometers and SAA, (b) horizontal displacement records measured by potentiometers and SAA, and (c) horizontal displacements based on motion tracking analysis of high speed digital video records taken during shaking tests, using TrackEye Motion Analysis software (PhotoSonics, Inc., Burbank, CA, 2009).

A comparison of the *x*-acceleration time histories (longitudinal) recorded by the traditional accelerometers placed on the laminates

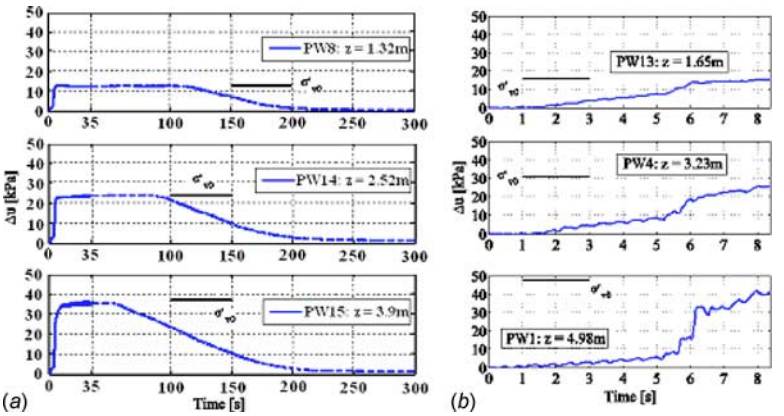


FIG. 15—*Excess pore pressure: (a) LG-0; (b) SG-1.*

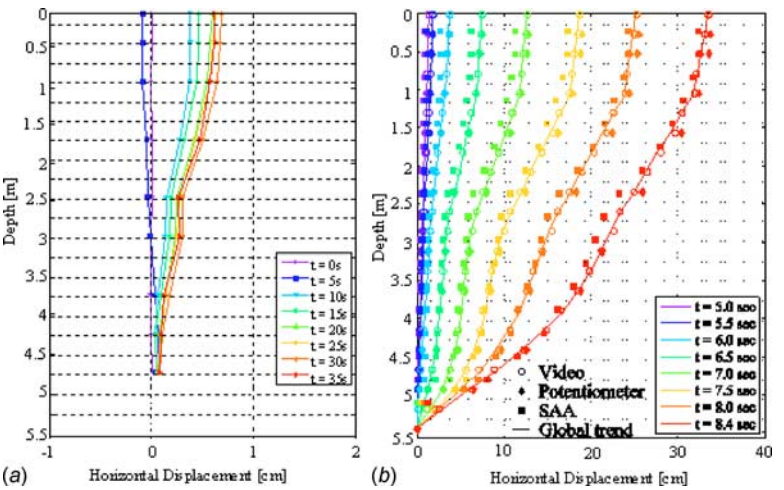


FIG. 16—*Horizontal displacement profiles: (a) LG-0; (b) SG-1.*

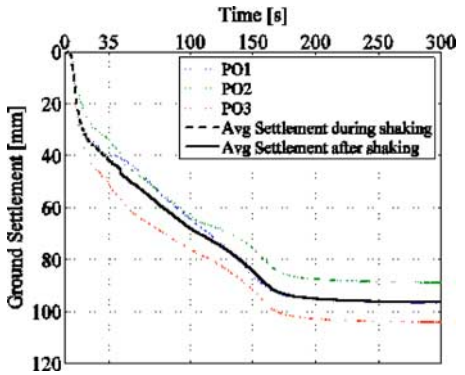


FIG. 17—*Settlement histories for LG-0.*

and SAA sensors at five different depths in SG-1 is shown in Fig. 18(*a*). Barring some minor differences, both arrays (accelerometers and SAA sensors) are in excellent agreement. Figure 18(*b*) shows a comparison between *x*-displacement time histories recorded by potentiometers and SAA sensors at the same depths in SG-1. The horizontal displacement recorded by the SAA sensor is in excellent agreement with that of the potentiometer. Figure 16(*b*) shows a comparison of horizontal displacement profile for SG-1, measured independently using potentiometers, SAA sensors, and video image analysis. All data corroborate each other very well. Such an agreement of comparisons of accelerations and displacement obtained from different types of sensors indicates that the recordings are of high quality and capture the actual response of the soil.

### *Utility of the Sensor Data*

The tests LG-0 and SG-1 involved more than 400 sensors in each case. Thus a wealth of high quality data is available to study the response of level and sloping grounds during seismic excitations and to understand liquefaction and lateral spreading phenomenon with a close scrutiny. In particular, these tests showed that despite nearly the same relative density of soils in both tests, the response of the deposit for SG-1 as evidenced in the very large displacements for SG-1 was very significantly different from that of the level ground deposit in LG-0. These subjects and the utility of the sensor data are treated in depth in a series of reports and papers elsewhere (Dobry et al. 2007; Bethapudi 2008; Gonzalez 2008; Ecemis 2008; Dobry et al. 2009; Bennett et al. 2009; El Shamy et al. 2009; Thevanayagam et al. 2009).

## Conclusions

Details of a 1-g laminar box system that can be used to perform large scale shake tests on soil models to study the phenomena of liquefaction and lateral spreading in gentle slopes have been presented. The system is capable of applying any desired base motion using two computer controlled actuators. Two tests were conducted to study the capabilities of this system to simulate liquefaction and lateral spreading phenomena in two nearly 5 m deep hydraulic fill deposits instrumented with a dense array of accelerometers, piezometers, potentiometers, high speed video cameras, and MEMS-type sensors. In both the tests, it was possible to prepare high quality loose sand deposit mimicking underwater sedimentation process that takes place in harbors, lakes, and river beds, which are generally prone to liquefaction. The laminar box system performed well. Significant horizontal displacements were observed for sloping ground test with a gentle slope. The high quality of the dense array instrumentation data was verified by cross-comparison between different types of sensors that measure the same quantity. Initial analyses of a limited data show that liquefaction occurred in both tests. Detailed analyses of the experiments, contrasting between the performance of level ground and gently sloping ground, and findings on mechanisms causing lateral spreading are presented elsewhere (Bethapudi 2008; Dobry et al. 2009).

### *Acknowledgments*

This material is based upon work supported by the National Science Foundation under Grant Nos. CMS-0529995, CMS-0086611, and CMS-0086612. This support is gratefully acknowledged. The authors wish to thank Thomas Albrechcinski, Jason Hanley, and the staff members of the UB-NEES site and Javier Ubilla and Hassan

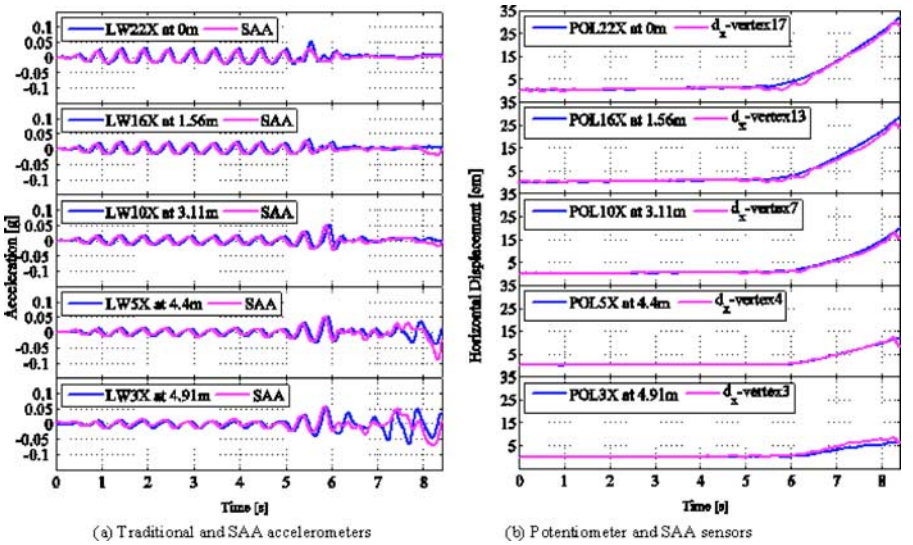


(a) Traditional and SAA accelerometers (b) Potentiometer and SAA sensors

FIG. 18—*Cross-comparison between different types of sensors (SG-1): (a) Traditional and SAA accelerometers; (b) potentiometer and SAA sensors.*

Radwan of the RPI-NEES site for their valuable support in experimentation and instrumentation. Special thanks are extended to graduate students V. Bennett, R. Bethapudi, M. Gonzalez, C. Medina, and T. Shenthan for their creative contributions toward this research.

## References

Abdoun, T., Bennett, V., Dobry, R., Thevanayagam, S., and Danisch, L., 2008, "Full-Scale Laboratory Tests Using a Shape-Acceleration Array System," ASCE Special Publication No. 181, Geotechnical Earthquake Engineering and Soil Dynamics, ASCE, Reston, VA, p. 9.

Abdoun, T. and Danisch, L., 2005, "Advanced Sensing for Real-Time Monitoring of Geotechnical Systems," *Proceedings of the Geo-Frontiers 2005 Conference*, Austin, TX, January 24–26, ASCE, Reston, VA.

Abdoun, T., Dobry, R., O'Rourke, T. D., and Goh, S. H., 2003, "Pile Response to Lateral Spreads: Centrifuge Modeling," *J. Geotech. Geoenviron. Eng.*, Vol. 129, No. 10, pp. 869–878.

Ashford, S. A., Juirnarongrit, T., Sugano, T., and Hamada, M., 2006, "Soil-Pile Response to Blast-Induced Lateral Spreading. I: Field Test," *J. Geotech. Geoenviron. Eng.*, Vol. 132, No. 2, pp. 152–162.

Bartlett, S. F. and Youd, T. L., 1992, "Empirical Analysis of Horizontal Ground Displacement Generated by Liquefaction-Induced Lateral Spreads," Technical Report No. NCEER-92-0021, National Center for Earthquake Engineering Research, Buffalo, NY.

Bennett, V., Abdoun, T., Danisch, L., Shantz, T., Jang, D., and Thevanayagam, S., 2009, "Design and Characterization of a Compact Array of High-Resolution MEMS Accelerometers for Instrumenting Soil and Soil-Structure Systems," *Smart Structures and Systems* (in press).

Berrill, J. B., Christensen, S. A., Keenan, R. J., Okada, W., and Pettinga, J. K., 1997, "Lateral-Spreading Loads on a Piled Bridge Foundation," *Seismic Behavior of Ground and Geotechnical Structures*, S. E. Pinto, Ed., Balkema, Rotterdam, The Netherlands, pp. 176–183.

Bethapudi, R., 2008, "Liquefaction-Induced Lateral Spreading in 1 g Full-Scale Shake Testing," M.S. thesis, Dept. of Civil, Structural, and Environmental Engineering, State University of New York at Buffalo, Buffalo, NY.

Brandenberg, S. J., Boulanger, R. W., Kutter, B. L., and Chang, D., 2005, "Behavior of Pile Foundations in Laterally Spreading Ground During Centrifuge Tests," *J. Geotech. Geoenviron. Eng.*, Vol. 131, No. 11, pp. 1378–1391.

Brandenberg, S. J., Boulanger, R. W., Kutter, B. L., and Chang, D., 2007, "Liquefaction-Induced Softening of Load Transfer Between Pile Groups and Laterally Spreading Crusts," *J. Geotech. Geoenviron. Eng.*, Vol. 133, No. 1, pp. 91–103.

Dobry, R. and Abdoun, T., 2001, "Recent Studies on Seismic Centrifuge Modeling of Liquefaction and Its Effect on Deep Foundation," *Proceedings of the Fourth International Conference on Recent Advances in Geotech. Earthq. Eng. and Soil Dyn.*, Vol. 2, San Diego, CA, March 26–31, S. Prakash, Ed., University of Missouri-Rolla Continuing Education, Missouri.

Dobry, R., Taboada, V., and Liu, L., 1995, "Centrifuge Modeling of Liquefaction Effects During Earthquakes," *Proceedings of the First International Conference on Earthq. Geotech. Eng. (IS-Tokyo)*, Keynote Lecture, Tokyo, Japan, A. A. Balkema, Rotterdam/Brookfield, pp. 1291–1324.

Dobry, R. and Taboada, V. M., 1994, "Possible Lessons from VELACS Model No. 2 Results," *Proceedings of the International Conference on Verification of Numerical Procedures for the Analysis of Soil Liquefaction Problems*, Vol. 2, K. Arulanandan and R. F. Scott, Eds., Balkema, Rotterdam, pp. 1341–1352.

Dobry, R., Thevanayagam, S., Abdoun, T., Elgamal, A., Elshamy, U., Zeghal, M., and Medina, C., 2007, "Study of Pile Response to Lateral Spreading Using Physical Testing and Computational Modeling," *Proceedings of the Fourth International Conference on Earthquake Geotechnical Engineering*, Thessaloniki, Greece.

Dobry, R., Thevanayagam, S., Medina, C., Bethapudi, R., Elgamal, A., Bennett, V., Abdoun, T., Zeghal, M., and ElShamy, U., 2009, "Mechanics of Lateral Spreading Observed in Full-Scale Shake Test," *J. Geotech. Geoenviron. Eng.* (unpublished).

Ecemis, N., 2008, "Effects of Permeability and Compressibility on Liquefaction Screening Using Cone Penetration Resistance," Ph.D. Dissertation, Dept. of Civil, Structural, and Environmental Engineering, State University of New York at Buffalo, Buffalo, NY.

El Shamy, U., Zeghal, M., Dobry, R., Thevanayagam, S., Elgamal, A., Abdoun, T., Medina, C., Bethapudi, R., and Bennett, V., 2009, "Micromechanical Aspects of Liquefaction-Induced Lateral Spreading," *Int. J. Geomech.* (unpublished).

Elgamal, A., Zeghal, M., Taboada, V., and Dobry, R., 1996, "Analysis of Site Liquefaction and Lateral Spreading Using Centrifuge Testing Records," *Soils Found.*, Vol. 36, No. 2, pp. 111–121.

Gonzalez, M. A., 2008, "Centrifuge Modeling of Pile Foundation Response to Liquefaction and Lateral Spreading: Study of Sand Permeability and Compressibility Effects Using Scaled Sand Technique," Ph.D. Thesis, Dept. of Civil and Environmental Engineering, Rensselaer Polytechnic Institute, Troy, NY.

Haigh, S. K. and Madabhushi, S. P. G., 2005, "The Effect of Pile Flexibility on Pile-Loading in Lateral Spreading Slopes," *Geotech. Spec. Publ.*, Vol. 145, R. W. Boulanger and K. Tokimatsu, Eds., pp. 24–37.

Hamada, M. and O'Rourke, T. D., 1992, "Case Studies of Liquefaction and Lifeline Performance During Past Earthquakes. Vol. 1: Japanese Case Studies," Tech. Report No. NCEER-92-0001, NCEER, SUNY-Buffalo, Buffalo, NY.

Hamada, M., Yasuda, S., Isoyama, R., and Emoto, K., 1986, "Study on Liquefaction Induced Permanent Ground Displacements," Research Report, Assn. for Development of Earthquake Prediction, Japan, November.

He, L., Elgamal, A., Abdoun, T., Abe, A., Dobry, R., Meneses, J., Sato, M., and Tokimatsu, K., 2006, "Lateral Load on Piles Due to Liquefaction-Induced Lateral Spreading During 1G Shake Table Experiments," *Proceedings of the Eighth U.S. National Conference on Earthq. Eng.*, Paper No. 881, San Francisco, CA, EERI, Oakland CA.

Ishihara, K., Yasuda, S., and Nagase, H., 1996, "Soil Characteristics and Ground Damage," *Soils Found.*, Special Issue: January, pp. 109–118.

Jamiolkowski, M., Lo Presti, D. C. F., and Manassero, M., 2001, "Evaluation of Relative Density and Shear Strength of Sands from CPT and DMT," Soil Behavior and Soft Ground Construc-

tion, *Geotech. Spec. Publ.*, Vol. 119, pp. 201–238, http://link.aip.org/link/?ASC/125/7/1.

Koyamada, K., Miyamato, Y., and Tokimatsu, K., 2005, "Field Investigation and Analysis Study of Damage Pile Foundation During the 2003 Tokachi-Oki Earthquake," *Geotech. Spec. Publ.*, Vol. 145, R. Boulanger and K. Tokimatsu, Eds., pp. 97–108.

Lambe, T. W. and Whitman, R. V., 1969, *Soil Mechanics*, Wiley, New Jersey.

Lancellotta, R., 1983, "Analisi di Affidabilita in Ingegneria Geotecnica," Atti dell'Istituto di Scienza delle Costruzioni No. 625, Politecnico di Torino (in Italian).

Lin, S., Tseng, Y., Chiang, C., and Hung, C., 2005, "Damage of Piles Caused by Lateral Spreading-Back Study of Three Cases," *Geotech. Spec. Publ.*, Vol. 145, R. W. Boulanger and K. Tokimatsu, Eds., pp. 121–133.

McCulloch, D. S. and Bonilla, M. G., 1970, "Effects of the Earthquake of March 27, 1964 on the Alaska Railroad," Professional Paper No. 545-D, U.S. Geological Survey, Reston, VA, http://pubs.er.usgs.gov/usgspubs/pp/pp545D.

Mizuno, H., 1987, "Pile Damage During Earthquakes in Japan (1923–1983)," *Proceedings of the ASCE Conference on Dynamic Response of Pile Foundations*, T. Nogami, Ed., ASCE, Reston, VA, pp. 53–77.

O'Rourke, T. D. and Hamada, M. (Eds.), 1992, "Case Studies of Liquefaction and Lifeline Performance During Past Earthquakes. Vol. 2: United States Case Studies," Tech. Report No. NCEER-92-0002, NCEER, SUNY-Buffalo, Buffalo, NY.

Photo-Sonics, Inc. (2009), Burbank, CA., http://www.photosonics.com/trackeye_software.htm

Radwan, H. and Abdoun, T., 2006, "3D Data Viewing of Centrifuge Physical Models," *Geotech Special Publ. Proc. GeoCongress 2006 Conference: Geotechnical Engineering in the Information Technology Age*, February 26–March 1, Atlanta, GA, D. J. DeGroot, J. T. DeJong, D. Frost, and L. G. Baise, Eds., ASCE, Reston, VA.

Schmertmann, J. H., 1976, "An Updated Correlation Between Relative Density $D_r$ and Fugro-Type Electric Cone Bearing $q_c$," DACW 39-76 M6646, Waterways Experiment Station.

Suzuki, H., Tokimatsu, K., Sato, M., and Abe, A., 2005, "Factor Affecting Horizontal Subgrade Reaction of Piles During Soil Liquefaction and Lateral Spreading," *Geotech. Spec. Publ.*, Vol. 145, R. Boulanger and K. Tokimatsu, Eds., pp. 1–10.

Swan, S. W., Flores, P. J., and Hooper, J. D., 1996, "The Manzanillo Mexico Earthquake of October 9, 1995," NCEES Bulletin, Quarterly Publication of NCEER, Vol. 10, No. 1.

Taboada, V., 1995, "Centrifuge Modeling of Earthquake-Induced Lateral Spreading in Sand Using a Laminar Box," Ph.D. Thesis, Dept. of Civil Engineering, Rensselaer Polytechnic Institute, Troy, NY.

Taboada, V. M. and Dobry, R., 1994, "Experimental Results of Model No. 2 at RPI," *Proceedings of the International Conference on Verification of Numerical Procedures for the Analysis of Soil Liquefaction Problems*, Vol. 1, K. Arulanandan and R. F. Scott, Eds., Balkema, Rotterdam, The Netherlands, pp. 277–294.

Tamura, S. and Tokimatsu, K., 2005, "Seismic Earth Pressure Acting on Embedded Footing Based on Large-Scale Shaking Table Tests," *Geotech. Spec. Publ.*, Vol. 145, R. W. Boulanger and K. Tokimatsu, Eds., pp. 83–96.

Thevanayagam, S., 2007a, "Intergrain Contact Density Indices for Granular Mixes—I: Framework," *Earthquake Eng. Eng. Vib.*, Vol. 6, No. 2, pp. 123–134.

Thevanayagam, S., 2007b, "Intergrain Contact Density Indices for Granular Mixes—II: Liquefaction Resistance," *Earthquake Eng. Eng. Vib.*, Vol. 6, No. 2, pp. 135–146.

Thevanayagam, S., Dobry, R., Bethapudi, R., Abdoun, T., Elgamal, A., El Shamy, U., Zeghal, M., Bennett, V., Ubilla, J., Medina, C., and Reinhorn, A., 2009, "1-g Physical Modeling of Liquefaction and Lateral Spreading of Gentle Slopes," *Geotech. Test. J.* (unpublished).

Thevanayagam, S., Shenthan, T., and Kanagalingam, T., 2003, "Role of Intergranular Contacts on Mechanisms Causing Liquefaction and Slope Failures in Silty Sands," Research Report No. 240.6 T338r 2003, U.S. Geological Survey, Dept. of Interior, https://igsrglib03.er.usgs.gov/ipac20/ipac.isp?session=1248Xl66G5396.4212&menu=search&aspect=subtab13&npp=15&ipp=20&spp=20&profile=r&ri=&term=thevanayagam&index=.AW&aspect=subtab13&term=&index=JTK&term=&index=.SW&term=&index=.TW&term=&index=.GW&x=15&y=12#focus.

Thevanayagam, S., Shenthan, T., Mohan, S., and Liang, J., 2002, "Undrained Fragility of Sands, Silty Sands and Silt," *J. Geotech. Geoenviron. Eng.*, Vol. 128, No. 10, pp. 849–859.

Tokimatsu, K., 1999, "Performance of Pile Foundations in Laterally Spreading Soils," *Proceedings of the Second International Conference on Earthquake Geotechnical Eng.*, Vol. 3, Lisbon, Portugal, P. S. E. Pinto, Ed., pp. 957–964.

Tokimatsu, K., Mizuno, H., and Kakurai, M., 1996, "Building Damage Associated with Geotechnical Problems," *Soils Found.*, JGS Special Issue: January, pp. 219–234.

Towhata, I., Sesov, V., Motamed, R., and Gonzalez, M., 2006, "Model Tests on Lateral Earth Pressure on Large Group Pile Exerted by Horizontal Displacement of Liquefied Sandy Ground," *Proceedings of the Eighth U.S. National Conference on Earthq. Eng., Paper No. 1227*, San Francisco, CA, EERI, Oakland, CA.

Yokoyama, K., Tamura, K., and Matsuo, O., 1997, "Design Methods of Bridge Foundations Against Soil Liquefaction and Liquefaction-Induced Ground Flow," *Proceedings of the Second Italy-Japan Workshop on Seismic Design and Retrofit of Bridges*, Rome, Italy, Public Works Research Institute (PWRI N. 3503), Japan, pp. 109–131.

Youd, T. L., 1993, "Liquefaction-Induced Damage to Bridges," Transportation Research Record. No. 1411, Transportation Research Board and the National Research Council, Washington, D.C., pp. 35–41.

Youd, T. L., et al., 2001, "Liquefaction Resistance of Soils: Summary Report from the 1996 NCEER and 1998 NCEER/NSF Workshops on Evaluation of Liquefaction Resistance of Soils," *J. Geotech. Geoenviron. Eng.*, Vol. 127, No. 10, pp. 817–833.

Zeghal, M. and Elgamal, A., 1994, "Analysis of Site Liquefaction Using Earthquake Records," *J. Geotech. Engrg.*, Vol. 120, No. 6, pp. 996–1017.